Icarus 218 (2012) 906–916

Contents lists available at SciVerse ScienceDirect

Icarus

journal homepage: www.elsevier.com/locate/icarus

# Differential melt scaling for oblique impacts on terrestrial planets

Oleg Abramov [a,*], Stephanie M. Wong [b], David A. Kring [c]

[a] US Geological Survey, Astrogeology Science Center, 2255 N. Gemini Dr., Flagstaff, AZ 86001, United States
[b] Lunar and Planetary Laboratory, 1629 E. University Blvd., The University of Arizona, Tucson, AZ 85721, United States
[c] Lunar and Planetary Institute, Universities Space Research Association, 3600 Bay Area Blvd., Houston, TX 77058, United States

ARTICLE INFO

*Article history:*
Received 7 September 2011
Revised 15 December 2011
Accepted 27 December 2011
Available online 12 January 2012

*Keywords:*
Impact processes
Geophysics
Earth
Moon
Mars

ABSTRACT

Analytical estimates of melt volumes produced by a given projectile and contained in a given impact crater are derived as a function of impact velocity, impact angle, planetary gravity, target and projectile densities, and specific internal energy of melting. Applications to impact events and impact craters on the Earth, Moon, and Mars are demonstrated and discussed. The most probable oblique impact (45°) produces ~1.6 times less melt volume than a vertical impact, and ~1.6 and 3.7 times more melt volume than impacts with 30° and 15° trajectories, respectively. The melt volume for a particular crater diameter increases with planetary gravity, so a crater on Earth should have more melt than similar-size craters on Mars and the Moon. The melt volume for a particular projectile diameter does not depend on gravity, but has a strong dependence on impact velocity, so the melt generated by a given projectile on the Moon is significantly larger than on Mars. Higher surface temperatures and geothermal gradients increase melt production, as do lower energies of melting. Collectively, the results imply thinner central melt sheets and a smaller proportion of melt particles in impact breccias on the Moon and Mars than on Earth. These effects are illustrated in a comparison of the Chicxulub crater on Earth, linked to the Cretaceous–Tertiary mass extinction, Gusev crater on Mars, where the Mars Exploration Rover Spirit landed, and Tsiolkovsky crater on the Moon. The results are comparable to those obtained from field and spacecraft observations, other analytical expressions, and hydrocode simulations.

Published by Elsevier Inc.

## 1. Introduction

Hypervelocity impact cratering events vaporize, melt, and shatter planetary surfaces. The absolute volumes and relative proportions of these materials can affect crater morphology and the nature of the crater fill and crater ejecta. The proportion of impact melt relative to impact breccias (with or without melt fragments) can affect the magnitude of gravity and magnetic anomalies generated by an impact structure due to differences in density and demagnetization, for example, as observed at the terrestrial impact crater Chicxulub (e.g. Pilkington et al., 1994). The proportion of impact melt and impact breccias can also affect planetary surface properties such as surface roughness and thermal inertia, which can be measured from orbit and are highly relevant for landers and rovers.

Previous studies have shown that the volume of generated impact melt and its proportion relative to fragmented rock increases with crater diameter (e.g., Ahrens and O'Keefe, 1977; Grieve and Cintala, 1992; Pierazzo et al., 1997). The volume of impact melt also varies as a function of gravity, so the melt volume associated with craters of similar size on each of the terrestrial planets may vary greatly. Grieve and Cintala (1997), for example, suggested that melt volume associated with similar-sized transient craters is nearly six times greater on Earth and Venus than on the Moon. Higher pre-impact surface temperatures can also increase the amount of impact melt, producing, for example, 1.25 times more melt on Venus than on Earth in craters of similar final diameters (Grieve and Cintala, 1997) and over two times the amount of melt in an impact event on Mercury than one on the Moon (Cintala, 1992).

Comparisons described above were derived from analytical expressions that assume a vertical impact trajectory and, thus, are limited to only a small proportion of the impacts that occur on a planet. The most probable trajectories have impact angles of 45° (Gilbert, 1893; Shoemaker, 1962) and impact events with even shallower inclinations are common. There is a number of observed craters with elliptical shapes and asymmetric ejecta patterns, indicative of an impact angle of less than 15° with respect to the target surface, on the Moon (e.g., Gault and Wedekind, 1978) and Mars (e.g., Strom et al., 1992).

Recently, computer codes have been developed that allow three-dimensional simulations of impact events and, thus, oblique impacts, to be investigated. One numerical study (Pierazzo and Melosh, 2000) used hydrocode modeling to determine the amount

* Corresponding author.
*E-mail address:* oabramov@usgs.gov (O. Abramov).

0019-1035/$ - see front matter Published by Elsevier Inc.
doi:10.1016/j.icarus.2011.12.022

of melt produced by impacts at various impact angles on Earth and showed that it decreases as the impact angle decreases. Although hydrocodes are invaluable tools for exploring complex impact processes and parameters including layered terrains, presence of volatiles, friction, and porosity, it is computationally prohibitive to run such simulations for every crater or impact of interest. We address this need by developing general analytical expressions which build upon classic impact experiments and analytical studies, as well as recent numerical hydrocode simulations, and apply them to explore the production of melt in oblique impact events on the Earth, Moon, and Mars as a function of several impact parameters.

## 2. Calculating impact melt volume

Schmidt and Housen (1987), building on the work of Schmidt (1980), Holsapple and Schmidt (1982), and Gault and Sonett (1982), developed scaling techniques for calculating crater dimensions during the excavation stage. In particular, they used both theoretical and experimental techniques to derive scaling laws based on crater growth histories, final crater shapes, and formation times. They defined the following "$\pi$-scaling" parameters using dimensional analysis:

Dimensionless crater volume, also termed cratering efficiency:

$$\pi_v = \frac{\rho_t V_{tc}}{m_p} \tag{1}$$

Dimensionless crater radius:

$$\pi_r = R_{tc}\left(\frac{\rho_t}{m_p}\right)^{1/3} \tag{2}$$

Gravity-scaled size of an impact event:

$$\pi_2 = \frac{3.22ga}{v^2} \tag{3}$$

where $R_{tc}$, $\rho_t$, $m_p$, $V_{tc}$, $g$, $a$, and $v$ are the apparent transient crater radius (measured at the level of the original pre-impact surface), target density, mass of projectile, transient crater volume, gravity, impactor radius, and impact velocity, respectively. In addition, Schmidt and Housen (1987) derived the following relationships from impact and explosion experiments in several materials, including dry sand, wet sand, and water:

$$\pi_v = C_v \pi_2^{-\gamma} \tag{4}$$

$$\pi_r = C_r \pi_2^{-\beta} \tag{5}$$

where $C_v$, $\gamma$, $C_r$, and $\beta$ are material-dependent scaling parameters. Schmidt and Housen (1987) suggested values of $C_v = 0.2$, $\gamma = 0.65$, $C_r = 0.8$, and $\beta = 0.22$, obtained from impact experiments in wet sand targets, as the best-estimate for large-scale cratering in rock. These values are generally consistent with a recent iSALE-3D hydrocode study of oblique impacts in frictional targets (Elbeshausen et al., 2009), which found $\gamma = 0.66$, $C_r = 0.77$, $\beta = 0.22$. Parameter $C_v$ was found to have a strong dependence on both impact angle and friction coefficient of the target, ranging from 0.14 for a 30° impact in a target with a friction coefficient of 0.7, to 1.19 for a vertical (90°) impact in a frictionless target. Assuming that large-scale hypervelocity impacts have some degree of friction, $C_v$ suggested by the Elbeshausen et al. (2009), ranging from 0.14 to 0.32 for a frictional coefficient of 0.7, is generally consistent with Schmidt and Housen (1987). For the remainder of the manuscript, we will use the Schmidt and Housen (1987) parameters for wet sand listed above, with the exception of using $\gamma = 0.66$, rather than 0.65, as suggested by Elbeshausen et al. (2009). Having $\gamma = 3\beta$ sets up the proportionality $V_{tc} \propto D_{tc}^3$, which simplifies the derivation. This minor adjustment of $\gamma$ is within $1\sigma$ error of the Schmidt and Housen (1987) data.

Assuming that the projectile is spherical, its mass can be rewritten in the form of density ($\rho_p$) times the volume:

$$m_p = \frac{\pi}{6}\rho_p D_p^3 \tag{6}$$

Substituting Eqs. (1) and (3) into Eq. (4), replacing the mass with Eq. (6), using the scaling parameters discussed above ($C_v = 0.2$, $\gamma = 0.66$), and solving for $V_{tc}$ gives a transient crater volume of

$$V_{tc} = 0.0765\frac{\rho_p}{\rho_t} D_p^{2.34} g^{-0.66} v^{1.3} \tag{7}$$

for vertical impacts. Eq. (7) differs slightly from a previous derivation (Pierazzo and Melosh, 2000), where the constant was erroneously given as 0.28, rather than 0.0765, which produced a transient crater volume that was ~4 times too large.

Note that the transient crater volume inversely scales with gravity, indicating that if densities, projectile diameter, and projectile velocity are held constant, a given impact would produce a larger crater in a lower-gravity environment. This is consistent with the understanding that it requires less energy to form a crater of a given diameter on lower-gravity worlds (e.g., Grieve and Cintala, 1997).

Both experimental studies (Gault and Wedekind, 1978) and hydrocode simulations (Pierazzo and Melosh, 2000; Elbeshausen et al., 2009) indicate that the volume of the transient crater decreases in an approximately sinusoidal manner (that is, as a function of $\sin\theta$) with decreasing impact angle. This angle dependence can be approximated by replacing the impact velocity in the cratering efficiency relationship (Eq. (4)) with its vertical component, $v\sin\theta$ (Chapman and McKinnon, 1986), where $\theta$ is defined as 90° for a vertical impact. It should be noted that this approximation may represent the upper limit of angle dependence (Artemieva et al., 2004; Elbeshausen et al., 2009). Using this approximation, the more general form of the transient crater volume is

$$V_{tc} = 0.0765\frac{\rho_p}{\rho_t} D_p^{2.34} g^{-0.66} v^{1.3} \sin^{1.3}\theta \tag{8}$$

Substituting Eqs. (2) and (3) into (5), replacing the mass with Eq. (6), and using the Schmidt and Housen (1987) parameters for wet sand ($C_r = 0.8$, $\beta = 0.22$), the diameter of the transient crater ($D_{tc}$) is

$$D_{tc} = 2R_{tc} = 1.16\left(\frac{\rho_p}{\rho_t}\right)^{1/3} D_p^{0.78} g^{-0.22} v^{0.44} \tag{9}$$

where $D_{tc}$ is measured at the level of the pre-impact surface. Note that $D_{tc}$ is exactly proportional to $V_{tc}^{1/3}$ (Eq. (7)).

The dependence of the transient crater diameter on the impact angle is unclear, but appears to be weak and target-dependent. A three-dimensional hydrocode study by Elbeshausen et al. (2009) suggests that there is no impact angle dependence in frictionless (hydrodynamic) targets, and the decrease of crater volume with decreasing impact angle is due solely to the decrease in crater depth. It is worth noting that the experimental study by Gault and Wedekind (1978) likewise described a decrease of the depth/diameter ratio with decreasing impact angle. As the frictional coefficient of the target is increased in the Elbeshausen et al. (2009) study, the transient crater diameter begins to weakly vary with impact angle, up to a maximum of $\sim(\sin\theta)^{1/5}$ for the maximum investigated frictional coefficient of 0.7. In the derivation presented here, we opt not to include impact angle dependence because (i) the relationship is weak even for high frictional coefficients, (ii) it is not clear what frictional coefficient is appropriate for large-scale hypervelocity impacts, and (iii) it is already included in Eq. (8),

**Table 1**
Parameters used in impact melting calculations.

| Planetary body | Gravity ($m/s^2$) | Target material | Target density ($kg/m^3$) | Specific internal energy of melting (J/kg) | Impact velocity (m/s) | Projectile density ($kg/m^3$) |
|---|---|---|---|---|---|---|
| Earth (continental crust) | 9.81 | Granite | 2674[a] | $(5.2 \times 10^6)$[a] | 17,000[b] | 3320 |
| Earth (oceanic crust) | 9.81 | Basalt | 2860[c] | $(9.0 \times 10^6)$[a*] | 17,000[b] | 3320 |
| Moon (highlands) | 1.61 | Anorthosite | 2940[d] | $(3.42 \times 10^6)$[e] | 14,000[b] | 3320 |
| Moon (mare) | 1.61 | Basalt | 2860[c] | $(9.0 \times 10^6)$[a*] | 14,000[b] | 3320 |
| Mars | 3.7 | Basalt | 2860[c] | $(9.0 \times 10^6)$[a*] | 9600[f] | 3320 |

[a] Pierazzo et al. (1997).
[b] Chyba (1991).
[c] Melosh (1989).
[d] Ahrens and O'Keefe (1977).
[e] Bjorkman and Holsapple (1987).
[f] Ivanov (2001).
[*] $E_m$ for dunite is used as best available estimate.

which likely represents an upper limit of angle dependence (Elbeshausen et al., 2009); including it in Eq. (9) as well would lead to an overestimate of angle dependence later in the derivation.

The amount of melt generated by a given impactor can be estimated using the following expression, derived by Bjorkman and Holsapple (1987) using dimensional analysis:

$$\frac{M_{melt}}{m_p} = k\left(\frac{v^2}{E_m}\right)^{3\mu/2} \tag{10}$$

where $M_{melt}$ is the total mass of melt produced, $E_m$ is the specific internal energy of the target at shock pressure that results in melting upon release (please refer to Bjorkman and Holsapple (1987) for a full definition; values for common lithologies are given in Table 1 and definitions of all variables are presented in Table 2), and $\mu$ is the velocity exponent, related to the $\pi$-group scaling parameter $\gamma$ as $\gamma = 3\mu/(2+\mu)$ (Schmidt and Housen, 1987). For $\mu = 2/3$, and, correspondingly, for $\gamma = 0.75$, the mass of melt generated by a given impactor would scale with its kinetic energy. However, both laboratory experiments (Schmidt and Housen, 1987) and numerical calculations (O'Keefe and Ahrens, 1993; Elbeshausen et al., 2009), advocate lower values of $\mu \approx 0.56$ and $\gamma \approx 0.66$ as best estimates for large-scale cratering in rock, which yields less-than-energy scaling. The constant $k$ can be estimated from the hydrocode results of Pierazzo et al. (1997), and appears to vary with $\mu$, with $k = 0.22$ for energy scaling ($\mu = 2/3$), and $k = 0.42$ for $\mu = 0.56$, which we will use here. This dependency is further supported by a CTH hydrocode study by Barr and Citron (2011), who report intermediate values of $\mu = 0.62$ and $k = 10^{-0.482} = 0.33$.

Eq. (10) is assumed to vary with impact angle as $\sin^{1.3}\theta$, based on a hydrocode study by Pierazzo and Melosh (2000), which indicated that the volume of melt was directly proportional to the volume of the transient crater (Eq. (8)) when impact angle was the only parameter varied. After implementing the angle correction, substituting recommended constants ($k = 0.42$ and $\mu = 0.56$), replacing $M_{melt}$ with $\rho_t V_{melt}$, and substituting Eq. (6) into Eq. (10), the result is a melt volume expression for a given impactor:

$$V_{melt} = 0.22 E_m^{-0.85} \frac{\rho_p}{\rho_t} D_p^3 v^{1.7} \sin^{1.3}\theta \tag{11}$$

To derive melt volume for a given crater, we make use of the $\pi$-group scaling laws introduced earlier. If Eq. (9) is solved for $D_p$ and substituted into Eq. (11), one finds:

$$V_{melt} = 0.12 E_m^{-0.85} \left(\frac{\rho_p}{\rho_t}\right)^{-0.28} D_{tc}^{3.85} g^{0.85} \sin^{1.3}\theta \tag{12}$$

Both Eqs. (11) and (12), and all other expressions derived in this work, are not unit-dependent and will work with any self-consistent system of units.

These equations provide two interesting perspectives on impact melting. Whereas the volume of impact melt in a crater of a specific diameter (a geologist's perspective) is a function of planetary gravity (Eq. (12)) and independent of impact velocity, the volume of impact melt produced by a projectile of a specific diameter (an astronomer's perspective) is independent of planetary gravity and is a function of impact velocity (Eq. (11)). Also, comparing Eqs. (11) and (12), we see that $V_{melt}$ has the same dependence on $\theta$ for impacts producing a specific transient crater diameter ($D_{tc}$), as for impacts of a specific projectile diameter ($D_p$). Consequently, it may be possible to estimate the angle of impact from the volume of melt associated with a particular crater.

The volumes generated by the above analytical expressions are total shock-melt volumes and include the fraction of melt that may be injected into the crater floor, but not the melt-bearing breccias that may be produced by frictional melting or during crater modification. The latter, however, are not a significant fraction of the melt associated with an impact crater (e.g., Lieger et al., 2009; Riller et al., 2010). It is also important to note that all calculations in this work were carried out using full precision of constants and exponents, with only the final answer being rounded off to the appropriate number of significant figures.

## 3. Comparison of the Moon, Mars, and Earth

Eqs. (11) and (12) can be used to compare the amount of melt produced in impacts and craters of various sizes on Mars, the Moon, and Earth as a function of gravity on each of these bodies, typical impact velocities, representative target lithologies, and impact angles.

### 3.1. Model parameters

Input parameters used in impact melting calculations are summarized in Table 1. As illustrated by Eqs. (11) and (12), impact melt volume for both a particular impactor and a particular crater varies as a function of specific internal energy of melting and planetary surface density, and, thus, planetary surface lithologies. Earth's continents are composed of granitic crust, while oceanic crust is basaltic, Mars' crust is dominated by basalt, and the Moon consists of anorthosite in the highlands and basalt in the mare. Since basalt is a major crustal lithology common to all three planetary bodies, we use it in some of the calculations to highlight the effects of planetary gravity and impact velocity as the target composition is kept constant. However, we also test granite and anorthosite for the Earth and the Moon, respectively, to investigate the effects of different crustal compositions on melt production.

For purposes of this comparison, we assume that a dunite projectile, with a density of 3320 $kg/m^3$, is striking the three target lithologies described above. Dunite is used because it

represents the average of possible impactor densities, which can be as high as 7850 kg/m$^3$ for an iron projectile (Buchwald, 1975) or as low as 600 kg/m$^3$ for an icy comet like Shoemaker–Levy 9 (Asphaug and Benz, 1996). This density is also typical for ordinary chondrites.

Impact velocities typical for each planetary body are used. We use average impact velocities rather than root mean square velocities, because the latter are less representative of typical impact velocity values (Chyba, 1991), and values for asteroids are used rather than those for long-period comets, because asteroid impacts represent ~90% of all impacts.

### 3.2. Melt volume generated by a given projectile

Melt volumes in basalt targets as a function of projectile diameter are shown in Fig. 1a. Impact velocity is the next most dominant variable after projectile diameter, and thus impacts on Earth produce the most melt. Interestingly, more melt is produced on the Moon than Mars, even though the Moon's diameter is only half that of Mars. This is a consequence of the Moon's location, which is much farther from the asteroid belt than Mars, and the vicinity of Earth's gravitational field, both of which result in much higher impact velocities compared to Mars. For similar-sized projectiles, ~2.6 times more melt is produced on the Earth than on Mars and ~1.4 times more than on the Moon.

When different lithologies are used for different planetary bodies, namely granite for Earth, anorthosite for the Moon, and basalt for Mars, the results noticeably change (Fig. 1b). Impacts on Earth still produce the most melt, followed by the Moon and Mars, but absolute melt volumes are higher for the Earth and especially for the Moon. In fact, melt volumes for the Moon are now just barely smaller than those for the Earth. This is mainly a

**Table 2**
Definitions of variables (in order introduced).

| Variable | Definition |
|---|---|
| $\pi_r$ | Dimensionless crater radius |
| $\pi_v$ | Cratering efficiency parameter |
| $\pi_2$ | Gravity-scaled size of an impact event |
| $V_{tc}$ | Volume of the transient crater (measured at pre-impact surface) |
| $R_{tc}$ | Radius of the transient crater (measured at pre-impact surface) |
| $D_{tc}$ | Diameter of the transient crater (measured at pre-impact surface) |
| $\rho_t$ | Density of the target material |
| $\rho_p$ | Density of the projectile material |
| $m_p$ | Mass of the projectile |
| $g$ | Acceleration due to gravity |
| $v$ | Impact velocity |
| $a$ | Radius of the projectile |
| $D_p$ | Diameter of the projectile |
| $C_v$, | $\pi$-scaling constant in the dimensionless crater volume expression |
| $\gamma$ | $\pi$-scaling exponent in the dimensionless crater volume expression |
| $C_r$ | $\pi$-scaling constant in the dimensionless crater radius expression |
| $\beta$ | $\pi$-scaling exponent in the dimensionless crater radius expression |
| $\theta$ | Angle of impact with respect to the surface; 90° is vertical |
| $M_{melt}$ | Mass of impact melt |
| $\mu$ | Velocity exponent, related to the $\pi$-group scaling parameter $\gamma$ |
| $E_m$ | Specific internal energy of melting of the target |
| $V_{melt}$ | Volume of impact melt |
| $D_{tr}$ | Diameter of the transient crater (measured rim-to-rim) |
| $D_f$ | Diameter of the final crater (measured rim-to-rim) |
| $D_Q$ | Transition diameter between simple and complex craters |
| $d_m$ | Average depth of melting |
| $C_p$ | Specific heat capacity |
| $T$ | Temperature |
| $T_s$ | Surface temperature |
| $z$ | Depth |
| $T_L$ | Liquidus temperature |
| $L_m$ | Latent heat of melting |
| $C_s$ | Bulk speed of sound in the target material |
| $v_m$ | Minimum impact velocity required for shock melting |

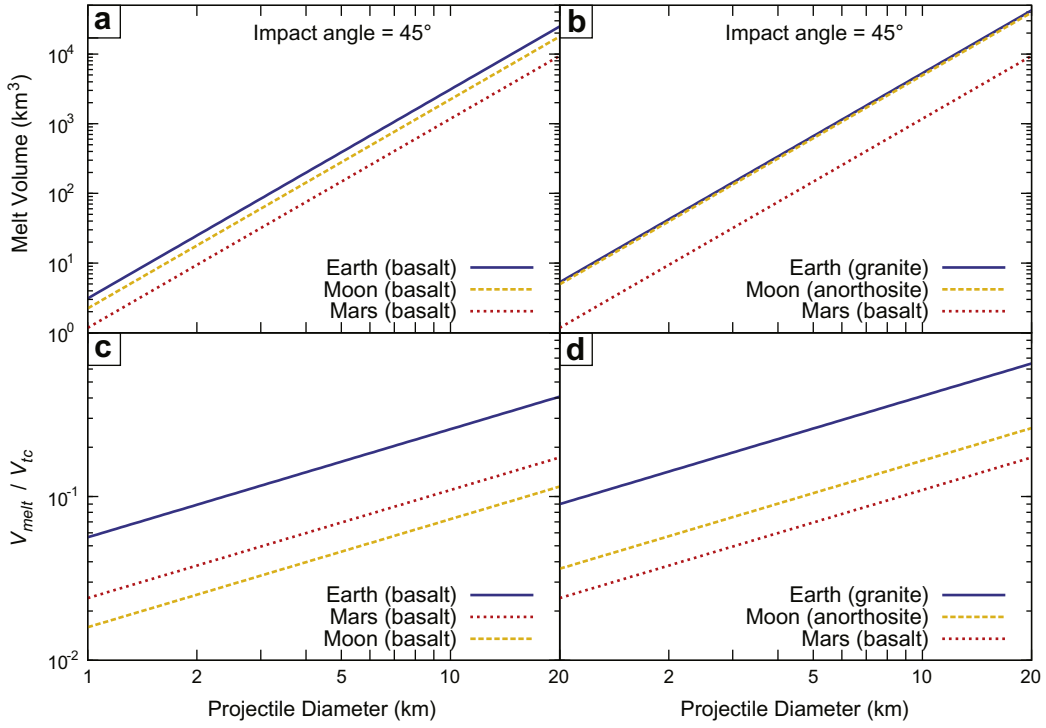


**Fig. 1.** Melt volumes and $V_{melt}/V_{tc}$ ratios for oblique 45° impacts as a function of projectile diameter on the Earth, Moon, and Mars, calculated with Eqs. (11) and (13). Impactor is an asteroid with a density of 3320 kg m$^{-3}$. (a) Melt volumes. Target is composed of basalt for all three planetary bodies. (b) Melt volumes. Target composition varies with planetary body: Earth – granite, Moon – anorthosite, and Mars – basalt. (c) Ratios of melt volume to transient crater volume. Target is composed of basalt for all three planetary bodies. (d) Ratios of melt volume to transient crater volume. Target composition varies with planetary body: Earth – granite, Moon – anorthosite, and Mars – basalt.

consequence of the different specific energies of melting (Table 1), with anorthosite requiring the least energy to melt, followed by granite and basalt. When different target lithologies are taken into account, impacts on Earth produce ~4.5 times more melt than on Mars and only a few percent more than on the Moon.

The ratio of melt volume to transient crater volume can be calculated as a function of projectile diameter by dividing Eq. (11) by Eq. (8):

$$\frac{V_{melt}}{V_{tc}} = 2.9E_m^{-0.85}D_p^{0.66}g^{0.66}v^{0.37} \quad (13)$$

This ratio inversely depends on $E_m$, because a material with a lower energy of melting will yield more melt, and $g$, because an impact of a given energy will yield a smaller crater in higher gravity. The dependence on $D_p$ and $v$ is likewise consistent, because both yield larger craters, which are known to have a higher proportion of melt based on observation evidence (e.g., Hawke and Head, 1977). There is no dependence on the impact angle, stemming from our earlier assumption that melt volume is directly proportional to transient crater volume (Eq. (8)) when impact angle is the only parameter varied (Pierazzo and Melosh, 2000).

The proportion of melt in a transient crater is far larger on Earth than on the Moon and Mars due to the combined influence of higher gravity and higher average impact velocity. This is illustrated in Fig. 1c and d, where $V_{melt}/V_{tc}$ is plotted as a function of projectile diameter. The value of $V_{melt}/V_{tc}$ on Earth is ~2.3 times that on Mars and ~3.5 times that on the Moon when basaltic targets are assumed, or 3.8 times that on Mars and 2.5 that on the Moon when different target lithologies are used. Consequently, whereas a crater produced by a 20-km diameter projectile on Earth is predicted to have a melt volume that is 40–65% of the transient crater volume, depending on assumed lithology, the predicted melt volume is only 17% that of the transient crater volume on Mars.

### 3.3. Melt volume in a given transient crater

As represented by Eq. (12), melt volume for a transient crater of a particular diameter is unaffected by impact velocity but increases with gravity. This effect is illustrated in Fig. 2a for the Earth ($g$ = 9.8 m/s$^2$), Mars ($g$ = 3.7 m/s$^2$), and the Moon ($g$ = 1.6 m/s$^2$), assuming an oblique impact angle of 45°, which is the most probable angle of impact. Within this scaling scheme, formation of a transient crater with a particular diameter on Earth generates ~2.3 times more melt than on Mars and ~4.6 times more melt than on the Moon, due solely to gravity.

When different lithologies are used for different planetary bodies, the results change somewhat (Fig. 2b). There is a weak dependence on density ratios (Eq. (12)), but the bulk of the change is due to the different specific internal energies of melting. Impacts on Earth still produce the most melt, followed by the Moon and Mars, as they did for the given impactor. Also, as before, absolute melt volumes are higher for the Earth and especially for the Moon due to lower energies of melting. When different target lithologies are taken into account, transient craters of a particular diameter on Earth contain ~3.6 times more melt than on Mars and ~3.2 times more than on the Moon.

As Eq. (9) indicates, similar-sized asteroids striking the Earth, Moon, and Mars produce different transient crater diameters, because of differential average impact velocity and the opposing effect of differential gravity. If the only variable were gravity, transient craters on Earth would be smaller than those on Mars. However, because the average impact velocity on Earth is

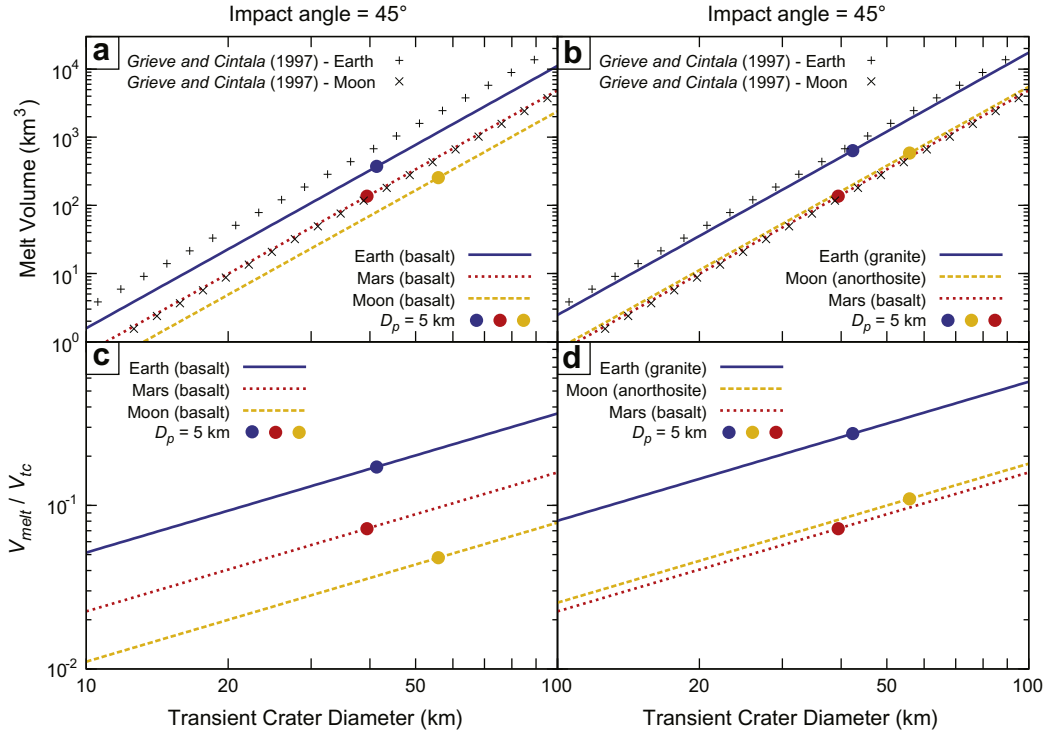


**Fig. 2.** Melt volumes and $V_{melt}/V_{tc}$ ratios for oblique 45° impacts as a function of transient crater diameter on the Earth, Moon, and Mars, calculated with Eqs. (12) and (14). Filled circles represent the transient crater diameter (Eq. (9)) and associated melt volume produced by a 5-km diameter asteroid with a density of 3320 kg m$^{-3}$. Grieve and Cintala (1997) results, corrected for the impact angle with $\sin^{1.3}\theta$, are shown for comparison. (a) Melt volumes. Target is composed of basalt for all three planetary bodies. (b) Melt volumes. Target composition varies with planetary body: Earth – granite, Moon – anorthosite, and Mars – basalt. (c) Ratios of melt volume to transient crater volume. Target is composed of basalt for all three planetary bodies. (d) Ratios of melt volume to transient crater volume. Target composition varies with planetary body: Earth – granite, Moon – anorthosite, and Mars – basalt.

significantly larger than on Mars, a transient crater produced on Earth is typically larger than that produced by a similar-sized projectile hitting Mars. This is illustrated with a 5-km diameter asteroid in Fig. 2, which consistently produces a larger transient crater on the Earth than on Mars, regardless of lithologies. The largest transient craters formed by this asteroid are on the Moon, because it has both low gravity and high average impact velocity. On the Moon a 5-km diameter asteroid will produce a 32–37% larger transient crater and 7–28% less melt, compared to the Earth, indicating vast differences between lunar and terrestrial craters. Not only is less melt produced on the Moon, a larger proportion of the material is excavated from a transient crater on the Moon and transported to crater distances farther from the point of impact. It should be noted, however, that the melt volume difference between lunar and terrestrial craters is less dramatic when final craters are considered, as discussed in Section 3.5.

The proportion of melt in a transient crater can also be calculated as a function of transient crater diameter by solving Eq. (9) for $D_p$, substituting it into Eq. (8), and dividing Eq. (12) by the result. This yields:

$$\frac{V_{melt}}{V_{tc}} = 2.5E_m^{-0.85}\left(\frac{\rho_p}{\rho_t}\right)^{-0.28} D_{tc}^{0.85} g^{0.85} \tag{14}$$

Thus, provided that projectile and target properties, as well as planetary gravity, are held constant, $V_{melt}/V_{tc}$ varies with $D_{tc}^{0.85}$, which is consistent with the finding by O'Keefe and Ahrens (1977) that the volume of melt relative to the volume of the crater should increase with final crater diameter at least as rapidly as $D_f^{0.55}$, or approximately $D_{tc}^{0.65}$ (please refer to Section 3.5 for conversion between transient and final crater diameters).

The ratio of melt volume to transient crater volume for a given transient crater (Fig. 2c and d) is similar to that for a given projectile (Fig. 1c and d). Earth consistently has the highest ratios, followed by either Mars when all targets are basaltic, or by the Moon when different lithologies are considered. The value of $V_{melt}/V_{tc}$ on Earth is ~2.3 times that on Mars and ~4.6 times that on the Moon when basaltic targets are assumed, or 3.6 times that on Mars and 3.2 that on the Moon when different target lithologies are used.

### 3.4. Melt volume as a function of impact angle

Using Eqs. (11) and (12), the volume of impact melt can be explored as a function of the impact angle between a projectile and planetary surface. As the trajectory becomes more oblique, the amount of target material that is shocked above the minimum pressure needed for melting decreases. It should also be noted, however, that the amount of shear heating within the target increases as the angle of impact becomes more oblique (e.g., Schultz, 1996). Nonetheless, at planetary scales, the effects of shear heating are probably limited to narrow shear bands localized near the surface along the projectile/target interface, which relieve differential stresses and are only a few centimeters to a few meters wide in large impacts (Pierazzo and Melosh, 2000). This implies relatively little melting due to shear heating.

For the purposes of comparison, a constant 5-km diameter projectile is assumed in Fig. 3. The target lithologies are held constant in Fig. 3a and vary in b. For all cases, about 1.6 times more melt is produced in a vertical impact than an oblique impact with a 45° trajectory, assuming all other parameters are constant. There is also 2.5 times more melt produced in an impact with a 90° trajectory than one with a 30° trajectory and that increases to 5.8 times more melt when compared to an oblique impact with a 15° trajectory. However, caution is urged when applying this scaling relationship to impacts at less than 30°, as several studies indicate that other processes that may affect melt volumes, such as projectile ricochet, occur at these shallow angles (e.g., Gault and Wedekind, 1978). As before, more melt is produced in terrestrial impact events than those on the Moon and Mars, with the same relative proportions as in Fig. 1a and b, which remain constant with impact angle.

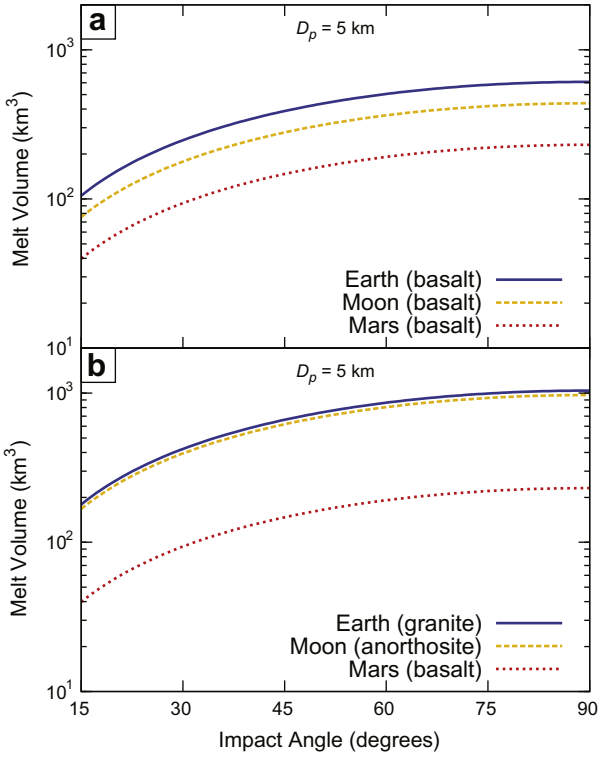


**Fig. 3.** Melt volume produced by a 5-km, 3320 kg m$^{-3}$ asteroid as a function of impact angle on the Earth, Moon, and Mars. Calculated with Eq. (11). (a) Target is composed of basalt for all three planetary bodies. (b) Target composition varies with planetary body: Earth – granite, Moon – anorthosite, and Mars – basalt.

### 3.5. Melt volume in a given final crater

The above results outline the geophysics of differential melt formation in oblique impacts, but do not readily lend themselves to geologic comparisons of similar-sized craters on each of the three planetary surfaces. To compare the volume of impact melt in craters of various final diameters (which are observable in images of planetary surfaces), we utilize a relationship between transient ($D_{tr}$) and final ($D_f$) rim-to-rim diameters, estimated using cumulative terrace widths, central uplift diameters, continuous ejecta radii, and transient crater reconstructions determined from lunar and terrestrial impact structures (Croft, 1985):

$$D_{tr} = D_Q^{0.15\pm0.04} D_f^{0.85\pm0.04} \tag{15}$$

where $D_Q$ is the simple-to-complex crater transition diameter, inversely proportional to gravity, ~3 km on Earth, ~8 km on Mars, and ~18 km on the Moon. These values are obtained from a least-squares fit of a $1/g$ line to data of Pike (1988). The transient crater diameter in this expression, $D_{tr}$, is a rim-to-rim measurement, whereas $D_{tc}$ used in $\pi$-scaling is measured at the level of the pre-impact surface. Thus, Eq. (15) needs to be modified by a factor of 1.2 (derived from data of Pike (1977)) to

$$D_{tc} = D_{tr}/1.2 = \left(D_Q^{0.15\pm0.04} D_f^{0.85\pm0.04}\right)\Big/1.2 \tag{16}$$

to be compatible with Eq. (12).

Fig. 4a and b plots melt volume as a function of final crater diameter for the most common (45°) oblique impact. These melt

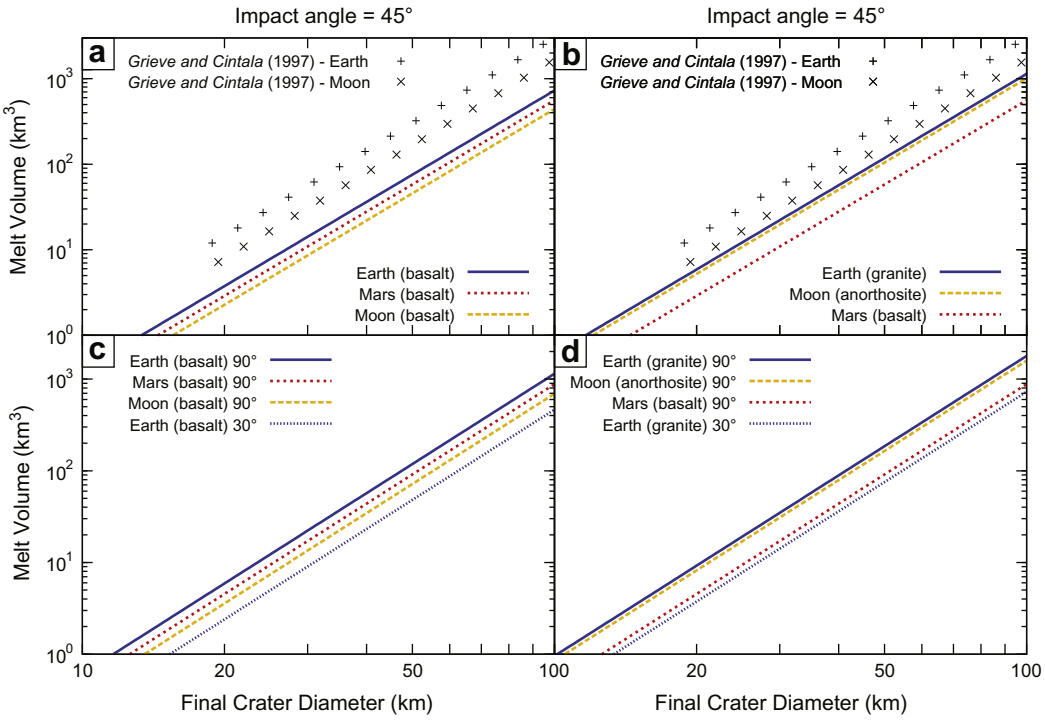


**Fig. 4.** Melt volumes for oblique impacts as a function of final crater diameter on the Earth, Moon, and Mars, calculated with Eqs. (12) and (16). Impactor is an asteroid with a density of 3320 kg m$^{-3}$. Results reported in Fig. 6 of Grieve and Cintala (1997), adjusted for the impact angle with $\sin^{1.3}\theta$, are shown for comparison. (a) 45° impacts. Target is composed of basalt for all three planetary bodies. (b) 45° impacts. Target composition varies with planetary body: Earth – granite, Moon – anorthosite, and Mars – basalt. (c) 30° and 90° impacts. Target is composed of basalt for all three planetary bodies. (d) 30° and 90° impacts. Target composition varies with planetary body: Earth – granite, Moon – anorthosite, and Mars – basalt.

volumes agree very well with the estimates for terrestrial craters by Ernst et al. (2010) using shock-heating calculations. When compared to melt volumes in transient craters in Fig. 2a and b, the general pattern is the same, but the most notable difference is that the disparity in melt volumes between the three bodies is less dramatic. For example, when basalt is used as a target lithology for all three bodies (Fig. 4a), a final crater of a given diameter on Earth contains only 1.3 times more melt than the one on Mars, and only 1.7 times more melt than the one on the Moon. This is due to the fact that for a given transient crater diameter, a larger final crater is formed on Earth than on Mars or the Moon (Eq. (16)) because higher gravity means more transient crater collapse during the modification stage. Thus, although terrestrial transient craters contain vastly more melt than Martian and lunar transient craters of the same size, they also yield larger final craters, which decreases the proportion of melt in the crater. Nonetheless, the difference in melt volumes is significant, and suggests, on the average, thinner central melt sheets in lunar and Martian craters, larger breccia to melt ratios, as well as a smaller proportion of impact melt particles in polymict breccias that fill or surround a crater.

If impact breccias on Mars and Moon contain, on the average, a smaller proportion of melt fragments than those on Earth, that implies the breccias are not as welded as they might be on Earth. A smaller volume of consolidated impact melt and a larger volume of relatively unconsolidated impact breccias on Mars and Moon will affect the evolution of regolith by making the subsurface rubbly and "broken-up".

Fig. 4c and d illustrates how the volume of impact melt varies as a function of final crater diameter on all three planets for other angles of impact. It can be seen that the melt produced in a 90° terrestrial impact will always be greater than that in impact events on the Moon and Mars, no matter the impact angle, for the same final crater size. The figures also show that melt volumes for 90° impacts on Moon and Mars are bracketed by melt volumes for the 30° and 90° impacts on the Earth. This implies that a given final crater on the Moon or Mars can easily have the same melt volume on as one on Earth.

### 3.6. Melt volumes in specific craters

To give a practical example, we compare three well-known craters, Chicxulub on Earth, Gusev on Mars, and Tsiolkovsky on the Moon, to illustrate the differences in the amount of melt produced on the three surfaces. These three craters were chosen because of their similar size. Gusev has a final crater diameter ($D_f$) of ~155 km, while Chicxulub is ~180 km, as is Tsiolkovsky. Eqs. (15) and (16) imply the rim-to-rim and apparent transient crater diameters are ~99 km and ~83 km for Gusev, ~97 km and ~81 km for Chicxulub, and ~127 km and ~106 km for Tsiolkovsky, respectively. Although Chicxulub and Gusev had similar transient crater diameters, they differ in final diameters due to the higher terrestrial gravity increasing the size of the crater during the modification stage, as previously discussed. To calculate the amount of melt from the two impacts, we used the same values given in Table 1 and assumed a 45° impact and different lithologies for each planetary body. This is consistent with the location of each crater, as Chicxulub formed in granitic continental crust, Tsiolkovsky is located in anorthositic lunar highlands, and Gusev is located in the basaltic southern highlands of Mars.

The amount of melt calculated for the Chicxulub, Gusev, and Tsiolkovsky craters is 7800 km$^3$, 2400 km$^3$, and 6900 km$^3$, respectively – a difference of over a factor of 3. These numbers, however, depend sensitively on the estimated transient crater diameter and assumed impact angle. For example, using the exponents at the upper limit of uncertainty in Eq. (16) results in an apparent transient crater diameter of 104 km and a melt volume of 21,000 km$^3$ for Chicxulub. Likewise, if an impact angle of 90° instead of 45° is used, melt volume for Chicxulub increases from 7800 km$^3$ to

12,000 km$^3$. Finally, accounting for pre-existing rock temperature at the average depth of melting can increase the melt estimate at Chicxulub by ~50% (Section 4).

This range agrees well with field observations at Chicxulub. For example, three-dimensional seismic tomography and gravity modeling suggests that the central melt sheet has a maximum thickness of 3–3.5 km in the center of the crater (Morgan et al., 2000; Ebbing et al., 2001). This is also consistent with the Pope et al. (2004) estimate of a 3.5 km central melt sheet at Chicxulub (with the caveat that the bottom 2.5 km may be a "melt breccia" that is only 65% melt) based on crater geometry and lithological data from boreholes. Seismic data by Morgan et al. (2000, 2002) also indicates that the central melt sheet terminates at the inner edge of the peak ring, and a separate melt sheet is present in the annular trough between the peak ring and the crater rim, which agrees with data from several boreholes drilled on either side of the peak ring (e.g., Kring et al., 2004). The maximum depth of the melt in the annular trough ranges from 250 to 500 m. The total volume of melt in the central melt sheet and the annular trough of the model crater is estimated from above sources to be 12,000 km$^3$ (Abramov and Kring, 2007) which is almost identical to the 12,631 km$^3$ proposed by Pope et al. (2004). This is a fairly robust estimate, generated from constraints imposed by crater geometry, seismic, gravity, and magnetic data, and four boreholes.

Constraining melt volumes at Gusev and Tsiolkovsky is more challenging. Tsiolkovsky, like most impact basins on the Moon, is filled with extensive mare basalts, making estimation of melt volume from orbital data difficult. The same holds true for Gusev. However, the basin of Tsiolkovsky has an area of an area of approximately 8500 km$^2$ (Tyrie, 1988), and thus our melt volume estimate corresponds to a maximum melt sheet thickness of ~1 km in the central regions of the crater.

## 4. Effects of target temperature

The temperature at the average depth of melting begins to play a progressively larger role with the increasing magnitude of the impact event, as well as with increasing surface temperature and/or geothermal gradient. For impacts on Venus, as well as impacts on Earth that are larger than approximately Chicxulub-sized, pre-impact rocks at the average depth of melting may already contain more than 50% of the energy needed to melt them, and this effect should be taken into account. If the initial melt volume is assumed to be roughly spherical in shape (e.g., Grieve and Cintala, 1997; Pierazzo and Melosh, 2000; Kring, 2005; Barr and Citron, 2011), the average depth of melting may be estimated as $d_m = (3V_{melt}/4\pi)^{1/3}$. For a given impactor (Eq. 11), this yields:

$$d_m = 0.37\left(E_m\left(1-\frac{C_p(T_s+\frac{dT}{dZ}d_m)}{C_pT_L+L_m}\right)\right)^{-0.28}\left(\frac{\rho_p}{\rho_t}\right)^{1/3} D_p\ v^{0.56} \times \sin^{0.44}\ \theta \quad (17)$$

For a given crater (Eq. 12), the result is:

$$d_m = 0.31\left(E_m\left(1-\frac{C_p(T_s+\frac{dT}{dZ}d_m)}{C_pT_L+L_m}\right)\right)^{-0.28}\left(\frac{\rho_p}{\rho_t}\right)^{-0.094} D_{tc}^{1.28}\ g^{0.28} \times \sin^{0.44}\ \theta \quad (18)$$

Please refer to Table 2 for definitions of variables. These equations are applicable only when the temperature at the average depth of melting is below the solidus, and temperatures are in Kelvin. The term $C_p(T_s+\frac{dT}{dz}d_m)$ represents the specific thermal energy of rocks at the average depth of melting, and the term $C_pT_L+L_m$ represents the specific thermal energy needed to melt the rocks. The ratio of these two terms represents the fraction of total energy of melting that is already present at depth. Eqs. (17) and (18) can be solved for $d_m$, which can then be used to evaluate the ratio described above and adjust $E_m$ in Eqs. (11) and (12) in the same way as in Eqs. (17) and (18). Fig. 5 shows the effect of temperature at the average depth of melting on melt volumes.

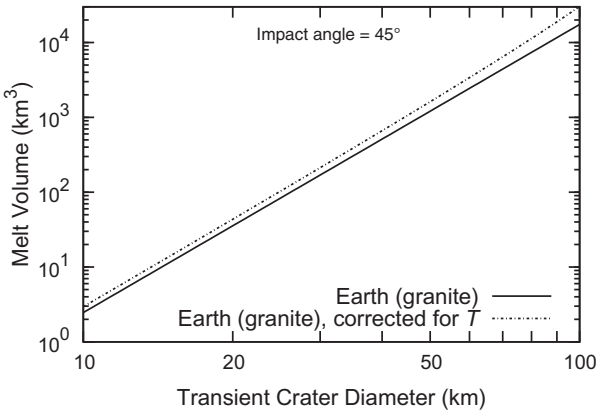


**Fig. 5.** Effects of target temperature at the average depth of melting on impact melt volume. Impactor is an asteroid with a density of 3320 kg m$^{-3}$. Solid line: melt volumes for oblique 45° impacts as a function of transient crater diameter on the Earth, calculated with Eq. (12). Dot-dash line: the above result corrected for pre-existing target temperature with Eq. (18). Heat capacity for granite at mid-crustal depths of 1200 J kg$^{-1}$ K$^{-1}$ (Waples and Waples, 2004), dry mid-crustal granite liquidus of 1373 K (Huang and Wyllie, 1973), granite latent heat of melting of 300 kJ/kg (e.g., Bittner and Schmeling, 1995), mean terrestrial surface temperature of 287 K (Jones et al., 1999), and average terrestrial geothermal gradient of 25 K km$^{-1}$ (Turcotte and Schubert, 1982) are used.

## 5. Comparisons to other analytical expressions for impact melt scaling

Perhaps the most commonly used analytical expression for differential melt scaling is that by Grieve and Cintala (1992, 1995, 1997), in which the melt volume is defined as $cD_{tc}^d$, where $c$ is a material-, velocity-, and gravity-dependent constant, and $d$ is a constant defined as 3.85 for all materials and impact velocities. The model presented in the present work validates, builds upon, and implements several improvements to that relationship. Comparing the Grieve and Cintala relationship to our expression for melt volume in a given transient crater (Eq. (12)), note that in both cases, melt volume scales as $D_{tc}^{3.85}$. Absolute melt volumes generated by Eq. (12) are also closely consistent, as illustrated by Fig. 2a and b, which contain results reported in Fig. 5 of Grieve and Cintala (1997). The best match is obtained in Fig. 2b, where we use a granite target for the Earth and an anorthosite target for the Moon, as did Grieve and Cintala (1997). We also confirm the conclusion of Grieve and Cintala (1997) that planetary gravity does not have any direct effect on melt generated by a given projectile (Eq. (11)), but affects the melt volume associated with a given transient crater (Eq. (12)).

However, our results also differ from those of Grieve and Cintala (1992, 1995, 1997) in several important respects. One is that our expression for melt volume in a given transient crater (Eq. (12)) does not have any impact velocity dependence, whereas constant $c$, and, therefore, the melt volume, in the Grieve and Cintala relationship increases weakly with impact velocity, likely because that derivation combined the Murnaghan equation of state, which assumes energy scaling (Kieffer and Simonds, 1980), with the Schmidt and Housen (1987) $\pi$-scaling relationship with parameters for wet sand, which yields less-than-energy scaling. Another difference between our work and that of Grieve and Cintala (1992, 1995, 1997) involves a dissimilarity in predicted melt

volumes in final craters, illustrated by Fig. 4a and b. This reflects our adjustment of crater diameters and, thus, melt volumes, as described in Eq. (16) and associated text.

Another common analytical expression for impact melt volume was derived by O'Keefe and Ahrens (1977) using estimates of shock-induced entropy increase in the target. For a given impactor:

$$V_{melt} = 1.3\frac{\rho_p}{\rho_t}D_p^3\left(\frac{v}{C_s}\right)^2 \tag{19}$$

where $C_s$ is bulk sound speed in the target. It compares well to our Eq. (11) in that both have the $\rho_p/\rho_t$ and $D_p^3$ terms, and neither has an explicit dependence on planetary gravity. The velocity exponent of 2 differs from our value of 1.7, due to the assumption of energy-scaling by O'Keefe and Ahrens (1977). The other difference is that the "ease of melting" of the target is accounted for indirectly using the bulk speed of sound, as opposed to directly using the specific internal energy of melting in Eq. (11).

O'Keefe and Ahrens (1977) also used the theoretical "$z$-model" of Maxwell (1977) and small-scale explosive experiment results of Ivanov (1976) to derive melt volume in a given final crater:

$$V_{melt} = \frac{5g^{0.553}}{\rho_t C_s^2}\left(\frac{D_f}{k}\right)^{3.55} \tag{20}$$

where $k$ is an empirical, material-dependent constant. It was not specified whether $D_f$ is a rim-to-rim or apparent crater diameter. Eq. (16) can be solved for $D_f$ and plugged into Eq. (20), with the result that $V_{melt}$ is proportional to $D_{tc}^{4.18}$ and $g^{1.18}$ for a given transient crater. This differs from our Eq. (12), which has $V_{melt}$ proportional to $D_{tc}^{3.85}$ and $g^{0.85}$, as well as from the Grieve and Cintala (1992, 1995, 1997) melt scaling expression. Other differences between Eqs. (12) and (20) include the lack of dependence on projectile density in Eq. (20), and the presence of an undefined material-dependent constant.

The final example of an analytical expression for impact melt volume is that of Tonks and Melosh (1993). It was derived using the Hugoniot equations, as well as experimentally-obtained shock- and particle-velocity relationship and shock attenuation as a function of distance:

$$V_{melt} = 0.52\frac{\rho_p}{\rho_t}D_p^3\left(\frac{v}{v_m}\right)^{3/2}\sin^{-1/2}\theta \tag{21}$$

where $v_m$ is the minimum impact velocity required for shock melting, and is dependent on target temperature and physical properties. Tonks and Melosh (1993) suggest $v_m$ values of 9.4 km/s for a dunite target at 298 K, and 7.1 km/s for a dunite target at 1490 K. This expression is similar in form to Eq. (11) in this paper, with melt volume scaling with $\rho_p/\rho_t$ and $D_p^3$ in both cases. Also, both relationships have less-than-energy scaling, with velocity exponents of 1.7 and 1.5 in Eqs. (11) and (21), respectively. The "ease of melting" of the target material is accounted for with the $v_m$ term in Eq. (21), whereas we use specific internal energy of melting ($E_m$) in Eq. (11). By far the most important difference, however, is that the $\sin\theta$ term has a negative exponent in Eq. (21), implying that the melt volume increases with the increasing obliquity of the impact. This contrasts with our results, as well as with hydrocode simulations (e.g., Pierazzo and Melosh, 2000; Ivanov and Artemieva, 2002), which indicate a decrease in melt volume with increasing impact obliquity.

In general, the present work represents several specific improvements and enhancements over previous efforts. We present internally consistent expressions for both a given crater and a given projectile, whereas the Grieve and Cintala (1992, 1995, 1997) expression is only valid for a given crater and the Tonks and Melosh (1993) expression is only valid for a given projectile. The expressions in this work explicitly contain all variable dependencies, rather than employing "catch-all" constants such as those in Grieve and Cintala (1992, 1995, 1997) and O'Keefe and Ahrens (1977), the numerical values for which are only given for a few conditions. In addition to broader applicability, our approach has the instructional value of illustrating how melt volumes depend on projectile and surface compositions, gravity, impact velocities, and impact angles. The usefulness of the expressions presented here is enhanced by an explicit correction for surface temperature and/or geothermal gradient, which makes them applicable to impacts of large magnitude or impacts on a hot world such as Venus. The expressions in this work are also self-consistent – one of the big issues in previous efforts has been mixing of energy-scaling and less-than-energy scaling expressions. Typically this involves the use of an energy-scaling method to calculate melt volume for a given projectile, and then the use of $\pi$-scaling with parameters for wet sand, which yields less-than energy scaling, to calculate melt volume in a given crater. Finally, and perhaps most importantly, we explicitly implement the dependence of melt volume on impact angle.

## 6. Comparisons to hydrocode-derived impact melt scaling

Eqs. (11) and (12) were derived from $\pi$-scaling and dimensional analysis, with the replacement of impact velocity in the cratering efficiency relationship with its vertical component as suggested by Chapman and McKinnon (1986). This analytical solution, however, yields somewhat different melt volumes and/or angle dependences over some oblique angles when compared to hydrocode simulations.

As represented by Fig. 6, CTH hydrocode simulations of impact events at five different impact angles (Pierazzo and Melosh, 2000) produced very similar, but not identical, results. Our melt volume estimate, obtained using the same parameters, is in very close agreement with their hydrocode-derived melt volume estimate for the 90° impact, assuming melting of the granite target at shock pressures of 50–60 GPa (Pierazzo et al., 1997). However, except for very oblique angles, our melt estimate decreases with $\theta$ faster than the hydrocode estimate, potentially resulting in underestimation of melt. This may be due to the approximation of an oblique impact as a vertical impact by simply taking its vertical velocity component, which neglects the energy delivered by the horizontal component of velocity. The hydrocode calculations, on the other

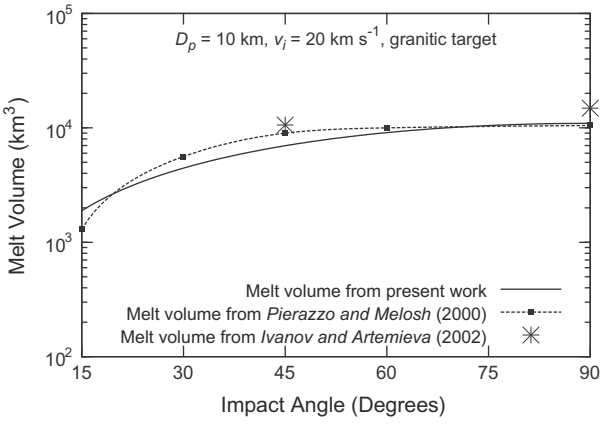


**Fig. 6.** Comparison of the melt volume estimates for an approximately Chicxulub-size impact generated by hydrocodes (Pierazzo and Melosh, 2000; Ivanov and Artemieva, 2002) to the analytical estimate presented in this paper. Projectile diameter is 10 km, impact velocity is 20 km/s. The impactor is dunite with a density of 3320 kg/m$^3$ and the target is granite with a density of 2674 kg/m$^3$. Calculated with Eq. (11). For the hydrocode results, melting of granite at 50 GPa was assumed (Pierazzo et al., 1997). No correction for target temperature is made in either hydrocode or analytical results.

hand, contain both components and indicate that the decrease of melt volume for oblique angles results from the slower average decay of the shock with distance from impact (Pierazzo and Melosh, 2000). This leads to the deposition of energy over a larger volume, decreasing peak shock pressures. Nonetheless, the analytical solution provides an acceptable approximation to the hydrocode results, and, if greater fidelity to the CTH hydrocode results is desired, the following variation of melt volume with $\theta$ may be used. Fitting the Pierazzo and Melosh (2000) hydrocode simulations explicitly for the melt volume generated by a given impactor,

$$V_{melt} \approx V_{melt,90} \sin^{C/\theta} \theta \quad (22)$$

where $V_{melt,90}$ is the melt volume for a vertical (90°) impact and $C$ is a constant that ranges from 25° for whole-rock melting at 50 GPa to 35° for whole-rock melting at 150 GPa.

Also shown in Fig. 6 are the results of a SOVA hydrocode simulation by Ivanov and Artemieva (2002). Although the absolute melt volumes are not in as close an agreement with our results as Pierazzo and Melosh (2000), the impact angle dependence is a much better match. This illustrates that two different hydrocodes can predict different impact angle dependencies given identical initial conditions.

We therefore present two options to the reader. To the extent one is confident in the impact angle dependence presented in this work, as well as in Ivanov and Artemieva (2002), Eqs. (11) and (12) provide good solutions. To the extent that one is confident in the impact angle dependence derived from Pierazzo and Melosh (2000) CTH hydrocode simulations (recently confirmed by Kraus et al. (2011), also with CTH) one can modify Eqs. (11) and (12) with Eq. (22).

## 7. Conclusions

We present here the first analytical expressions for the volume of melt produced by oblique impacts as a function of impact velocity, impact angle, planetary gravity, target and projectile densities, and specific internal energy of melting (Eqs. (11) and (12)). These expressions agree well with hydrocode simulations and may be modified as suggested if one desires to match the hydrocode results more precisely. In general, for similar-sized transient crater diameters and similar projectile diameters, impacts on Earth produce more impact melt than those on the Moon and Mars. For similar-sized transient crater diameters, a Martian impact produces more melt than a lunar impact (Fig. 2a), but for similar projectile diameters, an impact on the Moon creates more melt than one on Mars (Fig. 1a), if a basaltic target is assumed for all three planetary bodies. If different lithologies are used, however, with granite for Earth, anorthosite for the Moon, and basalt for Mars, a lunar transient crater is associated with more melt than a Martian one (Fig. 2b), due to the lower energy of melting of anorthosite compared to basalt. When comparing similar-sized final craters, there is expected to be more melt in the Chicxulub crater on Earth than the Tsiolkovsky crater on the Moon and the Gusev crater on Mars.

The most probable oblique impact angle is 45°, which produces 1.6 times less melt volume than a vertical impact and 3.7 times more melt volume than a very oblique 15° impact if all other variables are held constant. Although impact craters on the Earth are, on the average, expected to contain more melt, a crater formed by a 30° impact on the Earth would be expected to contain less melt than same size craters on the Moon and Mars formed by 90° impacts. The energy needed to melt material also has an appreciable effect on melt production. Because anorthositic and granitic crustal compositions require less energy to melt than basalts, this increases the amount of impact melt produced on the Moon and the Earth compared to Mars (Fig. 4b). Finally, higher surface temperatures and geothermal gradients increase melt production, and this effect becomes important on Earth for craters that are larger than approximately Chicxulub-sized.

## Acknowledgments

We thank the University of Arizona Summer Research Institute Program for sponsoring a portion of S.M.W.'s work in the NASA/Univ. Arizona Space Imagery Center. A portion of this work was supported by NASA Grant NAG510332 from the Planetary Geology and Geophysics Program, NASA Grant NAG512881 from the Cosmochemistry Program, and NASA Lunar Science Institute Contract NNA09DB33A to D.A.K. O.A.'s contribution to this work was sponsored by the Lunar and Planetary Institute through the Urey Fellowship program and NASA Grant NNX11AP57G from the Planetary Geology and Geophysics Program. D.A.K. also thanks Betty Pierazzo for reviewing and agreeing to the correction in Eq. (7). We thank Natalia Artemieva, Olivier Barnouin, Betty Pierazzo, Jennifer Anderson, and two anonymous reviewers for very thorough reviews of the current and previous versions of this manuscript. LPI Contribution # 1654.

## References

Abramov, O., Kring, D.A., 2007. Numerical modeling of impact-induced hydrothermal activity at the Chicxulub crater. Meteorit. Planet. Sci. 42, 93–112.
Ahrens, T.J., O'Keefe, J.D., 1977. Equations of state and impact-induced shock-wave attenuation on the Moon. In: Impact and Explosion Cratering. Pergamon Press, New York, pp. 639–656.
Artemieva, N., Karp, T., Milkereit, B., 2004. Investigating the Lake Bosumtwi impact structure: Insight from numerical modeling. Geochem. Geophys. Geosys. 5, Q11016.
Asphaug, E., Benz, W., 1996. Size, density, and structure of Comet Shoemaker–Levy 9 inferred from the physics of tidal breakup. Icarus 121, 25–248.
Barr, A.C., Citron, R.I., 2011. Scaling of melt production in hypervelocity impacts from high-resolution numerical simulations. Icarus 211, 913–916.
Bittner, D., Schmeling, H., 1995. Numerical modeling of melting processes and induced diapirism in the lower crust. Geophys. J. Int. 123, 59–70.
Bjorkman, M.D., Holsapple, K.A., 1987. Velocity scaling impact melt volume. Int. J. Impact Eng. 5, 155–163.
Buchwald, V.F., 1975. Handbook of Iron Meteorites: Their History, Distribution, Composition, and Structure. Univ. of California Press, Los Angeles.
Chapman, C.R., McKinnon, W.B., 1986. Cratering on planetary satellites. In: Burns, J.A., Matthews, M.S. (Eds.), Satellites. Univ. Arizona Press, Tucson, pp. 492–580.
Chyba, C., 1991. Terrestrial mantle siderophiles and the lunar impact record. Icarus 90, 217–233.
Cintala, M., 1992. Impact-induced thermal effects in the lunar and mercurian regoliths. J. Geophys. Res. 97 (E1), 947–973.
Croft, S.K., 1985. The scaling of complex craters. Proc. Lunar Sci. Conf. 15, 828–842.
Ebbing, J., Janle, P., Koulouris, J., Milkereit, B., 2001. 3D gravity modelling of the Chicxulub impact structure. Planet. Space Sci. 49, 599–609.
Elbeshausen, D., Wuennemann, K., Collins, G.S., 2009. Scaling of oblique impacts in frictional targets: Implications for crater size and formation mechanisms. Icarus 204, 716–731.
Ernst, C.M., Murchie, S.L., Barnouin, O.S., Robinson, M.S., Denevi, B.W., Blewett, D.T., Head III, J.W., Izenberg, N.R., Solomon, S.C., Roberts, J.H., 2010. Exposure of spectrally distinct material by impact craters on Mercury: Implications for global stratigraphy. Icarus 209, 210–223.
Gault, D.E., Sonett C.P., 1982. Laboratory simulation of pelagic asteroidal impact: Atmospheric injection, benthic topography, and surface wave radiation field. In: Silver, L.T., Schultz, P.H. (Eds.), Geological Implications of Impacts of Large Asteroids and Comets on the Earth, Special Paper 190. Geological Society of America, Boulder, pp. 137–175.
Gault, D.E., Wedekind J.A., 1978. Experimental studies of oblique impact. Proc. Lunar Sci. Conf. 9, 3843–3875.
Gilbert, G.K., 1893. The Moon's face. Bull. Philos. Soc. Wash. 12, 241–292.
Grieve, R.A.F., Cintala, M.J., 1992. An analysis of differential impact melt-crater scaling and implications for the terrestrial impact record. Meteoritics 27, 526–538.
Grieve, R.A.F., Cintala, M.J., 1995. Impact melting on Venus: Some considerations for the nature of the cratering record. Icarus 114, 68–79.
Grieve, R.A.F., Cintala, M.J., 1997. Planetary differences in impact melting. Adv. Space Res. 20, 1551–1560.
Hawke, B.R., Head, J.W., 1977. Impact melt in lunar crater interiors. Lunar Sci. VIII, 415–417.
Holsapple, K.A., Schmidt, R.M., 1982. On the scaling of crater dimensions 2. Impact processes. J. Geophy. Res. 87, 1849–1870.

Huang, W.L., Wyllie, P.J., 1973. Melting Relations of Muscovite-Granite at 35 kbar as a Model for Fusion of Metamorphosed Subdued Organic Sediments. Cont. Mineral. And Petrol. 42, 1–14.
Ivanov, B.A., 1976. The effect of gravity on crater formation: Thickness of ejecta and concentric basins. Proc. Lunar Sci. Conf. 7, 2947–2965.
Ivanov, B.A., 2001. Mars/Moon cratering ratio estimates. Space Sci. Rev. 60, 87–104.
Ivanov, B.A., Artemieva, N.A., 2002. Numerical modeling of the formation of large impact craters. Geol. Soc. Am. Special Paper 356, 619–630.
Jones, P.D., New, M., Parker, D.E., Martin, S., Rigor, I.G., 1999. Surface air temperature and its changes over the past 150 years. Rev. Geophys. 37, 173–199.
Kieffer, S.W., Simonds, C., 1980. The role of volatiles and lithology in the impact process. Rev. Geophys. Space Phys. 18, 143–181.
Kraus, R.G., Senft, L.E., Stewart, S.T., 2011. Impacts onto $H_2O$ ice: Scaling laws for melting, vaporization, excavation, and final crater size. Icarus 214, 724–738.
Kring, D.A., 2005. Hypervelocity collisions into continental crust composed of sediments and an underlying crystalline basement: Comparing the Ries (~24 km) and Chicxulub (~180 km) impact craters. Chemie der Erde 65, 1–46.
Kring, D.A., Zurcher, L., Hörz, F., Urrutia Fucugauchi, J., 2004. Impact lithologies and their emplacement in the Chicxulub impact crater: Initial results from the Chicxulub Scientific Drilling Project, Yaxcopoil, Mexico. Meteorit. Planet. Sci. 39, 879–897.
Lieger, D., Riller, U., Gibson, R., 2009. Generation of fragment-rich pseudotachylite bodies during central uplift formation in the Vredefort Impact Structure, South Africa. Earth Planet. Sci. Lett. 279, 53–64. doi:10.1016/j.epsl.2008.12.031.
Maxwell, D.E., 1977. Simple Z model of cratering, ejection and the overturned flap. In: Roddy, D.J., Pepin, R.O., Merrill, R.B. (Eds.), Impact and Explosion Cratering. Pergamon, NY, pp. 1003–1008.
Melosh, H.J., 1989. Impact Cratering: A Geologic Process. Oxford University Press, New York, 245pp.
Morgan, J.V., Warner, M.R., Collins, G.S., Melosh, H.J., Christeson, G.L., 2000. Peak ring formation in large impact craters: Geophysical constraints from Chicxulub. Earth Planet. Sci. Lett. 183, 347–354.
Morgan, J.V., Christeson, G.L., Zelt, C.A., 2002. Testing the resolution of a 3D velocity tomogram across the Chicxulub crater. Tectonophysics 355, 215–226.
O'Keefe, J.D., Ahrens, T.J., 1977. Impact-induced energy partitioning, melting, and vaporization on terrestrial planets. Proc. Lunar Sci. Conf. 8, 3357–3374.
O'Keefe, J.D., Ahrens, T.J., 1993. Planetary cratering mechanics. J. Geophys. Res. 98, 17001–17028.
Pierazzo, E., Melosh, H.J., 2000. Melt production in oblique impacts. Icarus 145, 252–261.
Pierazzo, E., Vickery, A.M., Melosh, H.J., 1997. A reevaluation of impact melt production. Icarus 127, 408–423.
Pike, R.J., 1977. Apparent depth/apparent diameter relations for lunar craters. Proc. Lunar Sci. Conf. 8, 3427–3436.
Pike, R.J., 1988. Geomorphology of impact craters on Mercury. In: Vilas, F., Chapman, C.R., Matthews, M.S. (Eds.), Mercury. Univ. Arizona Press, Tucson, pp. 165–273.
Pilkington, M., Hildebrand, A.R., Ortiz-Aleman, C., 1994. Gravity and magnetic field modeling and structure of the Chicxulub Crater, Mexico. J. Geophys. Res. 99, 13147–13162.
Pope, K.O., Kieffer, S.W., Ames, D.E., 2004. Empirical and theoretical comparisons of the Chicxulub and Sudbury impact structures. Meteorit. Planet. Sci. 39, 97–116.
Riller, U., Lieger, D., Gibson, R.L., Grieve, R.A.F., Stöffler, D., 2010. Origin of large-volume pseudotachylite in terrestrial impact structures. Geology 38, 619–622.
Schmidt, R.M., 1980. Meteor crater: Energy of formation–implications of centrifuge scaling. Proc. Lunar Sci. Conf. 9, 3877–3889.
Schmidt, R.M., Housen, K.R., 1987. Some recent advances in the scaling of impact and explosion cratering. Int. J. Impact Eng. 5, 543–560.
Schultz, P.H., 1996. Effect of impact angle on vaporization. J. Geophys. Res. 101, 21117–21136.
Shoemaker, E.M., 1962. Interpretation of lunar craters. In: Kopal, Z. (Ed.), Physics and Astronomy of the Moon. Academic Press, San Diego, pp. 283–359.
Strom, R.G., Croft, S.K., Barlow, N.G., 1992. The martian impact cratering record. In: Kieffer, H.H., Jakosky, B.M., Snyder, C.W., Matthews, M.S. (Eds.), Mars. Univ. Ariz. Press, Tucson, pp. 383–423.
Tonks, W.B., Melosh, H.J., 1993. Magma ocean formation due to giant impacts. J. Geophys. Res. 98, 5319–5333.
Turcotte, D.L., Schubert, G., 1982. Geodynamics: Applications of Continuum Physics to Geological Problems. John Wiley and Sons, New York, 450pp.
Tyrie, A., 1988. Description of the crater Tsiolkovsky on the lunar far side. Earth Moon Planets 42, 265–275.
Waples, D.W., Waples, J.S., 2004. A review and evaluation of specific heat capacities of rocks, minerals, and subsurface fluids. Part 1: Minerals and nonporous rocks. Nat. Resour. Res. 13, 97–122.